Meccanica (2012) 47:1705–1722
DOI 10.1007/s11012-012-9549-y

On the beneficial effect of rotor suspension anisotropy on viscous-dry hysteretic instability

Francesco Sorge · Marco Cammalleri

Received: 6 July 2011 / Accepted: 31 March 2012 / Published online: 17 April 2012

Abstract The destabilizing influence of the internal friction on the supercritical rotor whirl can be efficiently counterbalanced by other external dissipative sources and/or anisotropic suspension systems. The theoretical approach may take the internal dissipation into consideration either by dry or viscous models. Nevertheless, several numerical results and a new perturbation technique of the averaging type prove that similar rotor motions and stability limits are achievable by both models, whence the linear viscous assumption appears preferable. Thus, the internal hysteretic force may be expressed by the product of an equivalent viscous coefficient and the rotor centre velocity relative to a reference frame rotating with the shaft end sections. After calculating the natural frequencies and the response to dynamic imbalances, the stability of the steady motion is checked by the Routh-Hurwitz criterion, focusing the analysis on the individual influence of several characteristic properties, like the gyro structure, the stiffness anisotropy of the supports and their asymmetry, and searching for the external damping level needed for stability. A fairly interesting result is that the benefit of the suspension anisotropy is most effective for a symmetric rotor mounted at the shaft mid-span and decreases significantly on increasing the configuration asymmetry, even moderately. It is also observed how the stability may somehow be associated with the coupling between progressive and retrograde precession motions.

Keywords Conical rotor whirl · Viscous-dry hysteresis · Stability · Rotating machinery

F. Sorge (✉) · M. Cammalleri
Dipartimento di Ingegneria Chimica, Gestionale, Informatica, Meccanica, Università di Palermo, Viale delle Scienze, 90128 Palermo, Italy
e-mail: francesco.sorge@unipa.it

M. Cammalleri
e-mail: marco.cammalleri@unipa.it

1 Introduction

There are several sources of internal dissipation in a rotor-shaft-bearing system, the most important of which are identifiable with the shaft own hysteresis and the possible shrink fit relaxation. As well known, the internal friction may exert a destabilizing influence in the speed range above the first critical speed, whose consequences may become important in some applications, such as in long light drive-shafts where the hysteretic properties of the material, e.g. carbon/epoxy, are more remarkable than in common metallic materials (see [1]). In despite of this, the unstable hysteretic trend can be efficiently counterbalanced by other external dissipative sources that may be present in the installation. For example, recent researches of the authors show that, suspending the journal boxes elastically and providing them of dry friction surfaces normal to the shaft axis, which rub against the frame, a strong damping action can be exerted on the hysteretic motions, apart from achieving also an excellent contrast to the critical flexural speeds [2–5].

Many researchers have been involved in these problems in the past, dating from the first approaches of Refs. [6–8]. Among the numerous papers, Ref. [9] reports a valuable stability analysis of a rotor mounted on a hysteretic shaft at equal distance from the bearings, where the stability threshold is searched by the Routh-Hurwitz criterion depending on various system parameters. Many other analyses develop fairly indepth formulations, where also the system asymmetry, the gyroscopic effects and the anisotropy of the supports are taken into consideration, but they generally address single isolated example cases and do not cover wide operating ranges [10–21]. In other papers, the main focus is on the particular damping properties of the supports, characterized for example by hydrostatic bearings [22] or by polymeric viscoelastic suspensions, whose constitutive laws are to be optimized in the speed domain according to some stabilization requirements [23, 24]. Approaches in terms of finite elements are also widely present in literature (e.g. [25, 26]), together with more general well-grounded theoretical formulations taking into consideration various possible aspects [27, 28]. Nevertheless, what is missing in literature is a systematic analysis of the individual influences of the geometric, inertial and dissipative properties of the rotating system on the stability threshold and in particular the study of the remarkable decay of the system stability on moving the rotor away from the shaft mid-span.

The present analysis, which develops the preliminary results of Ref. [29], aims at this investigation, dealing with all the above effects and broadly addressing the conical whirling motions of an asymmetric unbalanced rotor-support assembly subject to gyroscopic effects, with different suspension stiffness and damping coefficients in the horizontal and vertical planes. The unbalance is considered both as static (eccentricity of the mass centre) and dynamic (skewness of the principal axes of inertia).

After deriving the Campbell diagrams and the elliptical paths of the rotor and the bearings by standard procedures, the stability of the steady motion is checked by the Routh-Hurwitz method and a thorough investigation is carried out on the particular influence of the gyro structure, of the stiffness anisotropy of the supports and of the system asymmetry. Differently from many previous approaches, the objective is not so much the limit speed of stability, as the level of external damping needed to prevent unstable conditions in the whole speed range. The instability phenomena can be conveniently prevented by differentiating the suspension stiffness in the horizontal and vertical planes, or in two orthogonal inflexion planes in general, which confirms the results of previous researches, but highlighting the strong influence of the rotor position along the shaft and of the other characteristics.

A very simple theoretical relation between the hysteresis factor and the elastic constants is calculable at the stability threshold of symmetric systems and it is possible to show how the beneficial stabilizing effect of anisotropy may be somehow associated with the coupling between progressive and retrograde precession motions.

The internal dissipation may be modelled either by viscous or by Coulombian friction depending mainly on the significance of the shaft hysteresis or of the shrink fit slackening. The non-linear friction case may be dealt with by numerical procedures or by perturbation approaches, e.g. of the Krylov-Bogoliubov type. However, it is provable that the stability conditions are just slightly influenced by the choice of the one or the other model for low friction levels, provided that some proper equivalence is defined for the two respective coefficients. On the other hand, the hysteretic coefficient may be considered as a function of the relative angular speed with respect to the shaft end sections, either of the equilibrium deflection or of the single precession motions, but this choice turns out to be irrelevant as regards the absolute stability threshold throughout the whole speed range.

2 Mathematical scheme

Figure 1 shows the rotor-suspension system and may be used as a reference for the notation. The approach is classical and similar to Refs. [2–5, 30]. The rotor is subject to a static unbalance, specified by the location of the mass centre C at some fixed eccentricity e from the intersection O_1 of the shaft axis with the rotor diametral plane, and to a dynamic unbalance, which may be schematized by two equal fictitious point masses m_d, symmetric with respect to O_1, lying on a meridian plane which does not contain C in general. The masses of the support are neglected.

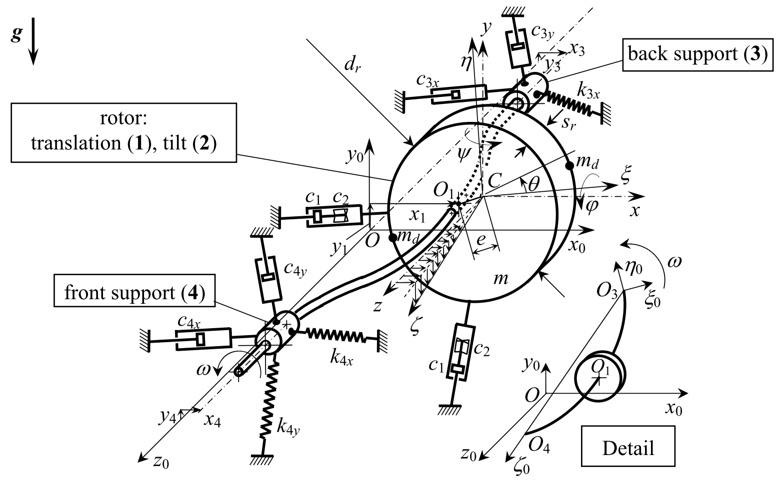

Fig. 1 Scheme of rotating machine. *Detail*: reference system rotating with driving end section

The frame $Cxyz$ moves with C remaining parallel to the fixed frame $Ox_0y_0z_0$, while the frame $C\xi\eta\zeta$ is obtainable by another auxiliary frame fixed to the rotor, through a backward rotation of the diametral axes ξ and η around ζ of an angle equal to the rotor rotation $\theta = \omega t$. Then, the reference $C\xi\eta\zeta$ does not partake in the main rotating motion with angular speed ω, but performs only the small rotations φ and ψ around the axes x and y due to the shaft deflection. Furthermore, the shaft is supposed horizontal and the gravitational field $\boldsymbol{g}$ is assumed directed towards $-y_0$.

The torsional deformation between the rotor and the end sections is ignored, as the torsional motion is uncoupled with the bending motion within the linear approximation.

The differentiation with respect to the dimensionless angular time variable $\theta = \omega t$ is indicated with primes, whence $\mathrm{d}(\ldots)/\mathrm{d}t = \omega(\ldots)'$, etc. Moreover, defining a reference shaft stiffness k_0 ($k_0 = 48EI/l^3$ for two self-aligning bearings, or $k_0 = 192EI/l^3$ for two cylindrical bearings, or $k_0 = 3EI/l^3$ for a cantilever shaft, where EI is the flexural stiffness and l the shaft length) and a reference critical speed $\omega_c = \sqrt{k_0/m}$, the angular speed ratio $\Omega = \omega/\omega_c$ may be introduced, together with the dimensionless stiffness ratios, $K_{3x} = k_{3x}/k_0$, $K_{3y} = k_{3y}/k_0$, $K_{4x} = k_{4x}/k_0$ and $K_{4y} = k_{4y}/k_0$, assuming different support stiffness in the horizontal and vertical planes. As regards the self-weight effects, the dimensionless gravity parameter $\Gamma = mg/(ek_0)$ is introduced.

Some external environmental dissipation is supposed to act on the rotor translational and rotational motions and the correspondent resistances are assumed viscous-like and linear for simplicity, whence the viscous equivalent coefficients c_1 [kg s^{-1}] and c_2 [kg m^2 s^{-1}] are introduced, together with the damping factors $d_1 = 0.5c_1\omega_c/k_0$ and $d_2 = 0.5c_2\omega_c/(k_0l^2)$. Similarly, the damping factors $d_{3x} = 0.5c_{3x}\omega_c/k_0$, $d_{3y} = 0.5c_{3y}\omega_c/k_0$, $d_{4x} = 0.5c_{4x}\omega_c/k_0$, $d_{4y} = 0.5c_{4y}\omega_c/k_0$, are ascribed to the horizontal and vertical damping of the suspension system, where the c's stand for viscous damping coefficients of the supports.

Similarly to [2–5], the shaft is considered massless, elastic and hysteretic, and the internal dissipative force acting on the rotor is assumed opposite to the velocity $\mathbf{v}_{\text{rel.}}$ of point O_1 relative to a reference system $O_3\xi_0\eta_0\zeta_0$ having the coordinate axis ζ_0 through the centres of the shaft end sections and rotating with the driving end section at the same angular speed ω (see detail of Fig. 1). In the case of two supports, indicating with $L_3 = -z_3/l$ and $L_4 = z_4/l$ the dimensionless distances of the rotor from the shaft ends, the components of $\mathbf{v}_{\text{rel.}}$ in the fixed reference $Ox_0y_0z_0$ are $v_{\text{rel.},x} = \dot{x}_1 - \dot{x}_3L_4 - \dot{x}_4L_3 + \omega(y_1 - y_3L_4 - y_4L_3)$ and $v_{\text{rel.},y} = \dot{y}_1 - \dot{y}_3L_4 - \dot{y}_4L_3 - \omega(x_1 - x_3L_4 - x_4L_3)$, while for a cantilever shaft clamped at 3 and loaded at 4, they are $v_{\text{rel.},x} = \dot{x}_1 - \dot{x}_3 + \omega(y_1 - y_3)$ and $v_{\text{rel.},y} = \dot{y}_1 - \dot{y}_3 - \omega(x_1 - x_3)$. In the hypothesis of viscous-like friction, the hysteresis force may be expressed by use of a hysteretic coefficient c_h, $\mathbf{F}_h = -c_h \mathbf{v}_{\text{rel.}}$, and the forces on the supports are $\mathbf{F}_{3h} = -L_4 \mathbf{F}_h$, $\mathbf{F}_{4h} = -L_3 \mathbf{F}_h$, or else $\mathbf{F}_{3h} = -\mathbf{F}_h$ for a cantilever shaft. Assuming Coulomb friction, a different model must be applied: $\mathbf{F}_h = -F_{h,\text{dry}} \mathbf{v}_{\text{rel.}}/|\mathbf{v}_{\text{rel.}}|$, where $F_{h,\text{dry}}$ is the friction force level.

Considering the steady rotation of a perfectly balanced horizontal rotor, the shaft deflection plane is motionless and counter-rotates with opposite angular speed with respect to the mobile frame $O_3\xi_0\eta_0\zeta_0$. Therefore, point O_1 describes a circular path in this frame and the hysteretic work per single revolution is given by the integral $c_h \oint (v^2_{\text{rel.},x} + v^2_{\text{rel.},y})\text{d}t = c_h\omega \oint [(y_1 - L_4 y_3 - L_3 y_4)^2 + (-x_1 + L_4 x_3 + L_3 x_4)^2]\text{d}\theta$, where x_j and y_j are equilibrium values. Assuming that this cyclic work is proportional to the square of the path radius and independent of ω, the product $c_h\omega$ turns out to be constant and a constant hysteresis factor $d_h = 0.5 c_h \omega / k_0$ may be introduced (see [31]).

The presence of some unbalance induces a further rotating bending with the same angular speed of the shaft and, in the case of isotropic stiffness and damping of the supports ($K_{3x} = K_{3y}$, $K_{4x} = K_{4y}$, $d_{3x} = d_{3y}$, $d_{4x} = d_{4y}$), this motion is circularly polarized, rigid with the frame $O_3\xi_0\eta_0\zeta_0$ and uninfluential on the overall friction work. For anisotropic suspension on the contrary, the trajectories are elliptical and passing from the fixed to the rotating frame $O_3\xi_0\eta_0\zeta_0$, they exhibit double looped shapes and are covered by twice the shaft frequency (2ω), because the radius vector is subject to increasing and decreasing phases twice during one full revolution of the rotating frame.

Following [31], the two mentioned dissipative cycles must be dealt with separately and two different hysteresis coefficients c_h must be defined, the one, c_{h1}, for the frequency ω and the other, c_{h2}, for the double frequency 2ω. As it is reasonable to assume that $\omega c_{h1} = 2\omega c_{h2} = h$ [31], where h is a hysteresis constant of the material, two hysteresis factors must be introduced, $d_{h1} = 0.5h/k_0$ for the relative rotation of the equilibrium deflection plane and $d_{h2} = 0.25h/k_0 = d_{h1}/2$ for the elliptical motions due to the unbalance. When applying some perturbation procedure to check the system stability, very small deviations of the perturbed trajectories from the steady paths are to be assumed and the factor d_{hi} may be kept unmodified. The use of the first or the second hysteresis factor in the stability analysis will depend on the prevalence of the gravity or the unbalance effect on the rotor response, $\Gamma = mg/(ek_0) > 1$ or $\Gamma = mg/(ek_0) < 1$.

If the dry friction internal dissipation has to be regarded as predominant in the system, the work per cycle is $F_{h,\text{dry}} \oint \sqrt{v^2_{\text{rel.},x} + v^2_{\text{rel.},y}}\text{d}t$ and a dry damping factor must be defined: $d_{h,\text{dry}} = F_{h,\text{dry}}/(k_0 e)$. The equivalence between dry and viscous friction can be stated and checked on the basis of the same energy dissipation during a sufficiently large number of revolutions and the parameters $d_{h,\text{dry}}$ and d_h can be thus correlated with each other.

It is convenient to scale all displacements by the rotor eccentricity e and all rotations by e/l and, using capital letters for dimensionless quantities, introduce the dimensionless displacement-rotation vectors, $\mathbf{X} = \{X_1, X_2, X_3, X_4\}^T$, $\mathbf{Y} = \{Y_1, Y_2, Y_3, Y_4\}^T$, where, using the subscripts 1, 3, 4 for the displacements of the rotor and the support and 2 for the rotor tilt around y and x, $X_j = x_j/e$, $Y_j = y_j/e$, for $j \neq 2$, $X_2 = \psi l/e$, $Y_2 = -\varphi l/e$ (the minus sign in the definition of Y_2 permits using the same form of the stiffness matrix for both the bending planes, xz and yz).

Scaling all forces and moments by $k_0 e$ and $k_0 e l$ respectively, introducing the dimensionless stiffness matrices K_{jz} in the inflexion planes xz $(j = x)$ and yz $(j = y)$, e.g.

$$\mathbf{K}_{jz} = \frac{1}{16 L_3^3 L_4^3} \begin{bmatrix} 1 - 3L_3 L_4 & L_3 L_4 (L_3 - L_4) & -L_4^3 & -L_3^3 \\ L_3 L_4 (L_3 - L_4) & L_3^2 L_4^2 & L_3 L_4^3 & -L_4 L_3^3 \\ -L_4^3 & L_3 L_4^3 & 16 L_3^3 L_4^3 K_{3j} + L_4^3 & 0 \\ -L_3^3 & -L_4 L_3^3 & 0 & 16 L_3^3 L_4^3 K_{4j} + L_3^3 \end{bmatrix} \tag{1}$$

for self-aligning bearings, and the hysteretic matrices $\mathbf{H}_i$ for $i = 1$ or 2 (frequency ω or 2ω)

$$\mathbf{H}_i = d_{hi} \begin{bmatrix} 1 & 0 & -L_4 & -L_3 \\ 0 & 0 & 0 & 0 \\ -L_4 & 0 & L_4^2 & L_3 L_4 \\ -L_3 & 0 & L_3 L_4 & L_3^2 \end{bmatrix} \tag{2}$$

the equations of motion can be written in the form

$$\mathbf{K}_{xz}\mathbf{X} + 2\Omega\mathbf{D}_{xz}\mathbf{X}' + 2\mathbf{H}_i(\mathbf{X}' + \mathbf{Y}) + \Omega^2\mathbf{M}\mathbf{X}'' + \Omega^2\mathbf{G}\mathbf{Y}' - \begin{Bmatrix} \Omega^2\cos\theta \\ -M_d\Omega^2\cos(\theta - \gamma) \\ 0 \\ 0 \end{Bmatrix} = 0 \tag{3a}$$

$$\mathbf{K}_{yz}\mathbf{Y} + 2\Omega\mathbf{D}_{yz}\mathbf{Y}' + 2\mathbf{H}_i(\mathbf{Y}' - \mathbf{X}) + \Omega^2\mathbf{M}\mathbf{Y}'' - \Omega^2\mathbf{G}\mathbf{X}' - \begin{Bmatrix} \Omega^2\sin\theta - \Gamma \\ -M_d\Omega^2\sin(\theta - \gamma) \\ 0 \\ 0 \end{Bmatrix} = 0 \tag{3b}$$

where $M_d = 0.5 m_d s_r d_r / elm$ is the dynamic unbalance parameter, s_r and d_r being the axial size and the diameter of the rotor (see Fig. 1), and γ is the angle between the meridian planes through C and through the point masses m_d. Moreover, $J_d = j_d/ml^2$ and $J_a = j_a/ml^2$ are the dimensionless diametral and axial moment of inertia of the rotor, scaled by the product ml^2, j_d and j_a being the real moment of inertia, evaluated in the absence of dynamic unbalance, and the matrices $\mathbf{D}_{jz}$ $(j = x, y)$, $\mathbf{M}$ and $\mathbf{G}$ of Eqs. (3a) and (3b) are diagonal and are the viscous, massive and gyroscopic matrices, whose coefficients are $(d_1, d_2, d_{3j}, d_{4j})$, $(1, J_d, 0, 0)$ and $(0, J_a, 0, 0)$ respectively.

Here, the first, third and fourth equations of (3a) and (3b) were made dimensionless dividing by ke (force equations), while the second equations were divided by kel (moment equations).

3 General results

The equilibrium configuration is obtained rewriting Eqs. (3a) and (3b) in the form $\mathbf{K}_{xz}\mathbf{X}_{\text{eq.}} + 2\mathbf{H}_1\mathbf{Y}_{\text{eq.}} = 0$, $\mathbf{K}_{yz}\mathbf{Y}_{\text{eq.}} - 2\mathbf{H}_1\mathbf{X}_{\text{eq.}} = -\Gamma\{1, 0, 0, 0\}^T$. This algebraic system leads to the solution, $\mathbf{X}_{\text{eq.}} = 2\mathbf{A}_{xz}\mathbf{H}_1(\mathbf{K}_{yz} + 4\mathbf{H}_1\mathbf{A}_{xz}\mathbf{H}_1)^{-1}\Gamma\{1, 0, 0, 0\}^T$, $\mathbf{Y}_{\text{eq.}} = -(\mathbf{K}_{yz} + 4\mathbf{H}_1\mathbf{A}_{xz}\mathbf{H}_1)^{-1}\Gamma\{1, 0, 0, 0\}^T$, where $\mathbf{A}_{jz} = \mathbf{K}_{jz}^{-1}$ are the flexibility matrices, and introducing the 2×2 shaft flexibility sub-matrix $[A_0]$ (fixed supports)

$$\mathbf{A}_0 = 16 \begin{bmatrix} L_3^2 L_4^2 & L_3 L_4(L_4 - L_3) \\ L_3 L_4(L_4 - L_3) & 1 - 3L_3 L_4 \end{bmatrix}$$

the solution is

$$\mathbf{X}_{\text{eq.}} = \frac{2d_{h1}\Gamma A_{0,11}}{1 + 4d_{h1}^2 A_{0,11}^2} \begin{Bmatrix} A_{0,11} \\ A_{0,21} \\ 0 \\ 0 \end{Bmatrix} \tag{4a}$$

$$\mathbf{Y}_{\text{eq.}} = -\Gamma \begin{Bmatrix} \frac{A_{0,11}}{1+4d_{h1}^2 A_{0,11}^2} + \frac{L_3^2}{K_{4y}} + \frac{L_4^2}{K_{3y}} \\ \frac{A_{0,21}}{1+4d_{h1}^2 A_{0,11}^2} - \frac{L_4}{K_{3y}} + \frac{L_3}{K_{4y}} \\ \frac{L_4}{K_{3y}} \\ \frac{L_3}{K_{4y}} \end{Bmatrix} \tag{4b}$$

As $X_{1\text{eq.}}$ and $X_{2\text{eq.}}$ are positive for $d_{h1} \neq 0$, while $X_{3\text{eq.}} = X_{4\text{eq.}} = 0$, the hysteresis appears to produce a static bias of the inflexion plane, concordant with the angular speed, while the static support deflection occurs in the vertical plane. Equations (4a) and (4b) show also that the static rotor displacement is small of order d_{h1} in the horizontal direction, whereas the changes of the vertical displacement due to hysteresis are of order d_{h1}^2.

The natural precession modes of the rotor-shaft system are obtainable ignoring the forcing terms in Eqs. (3a) and (3b) and putting $\mathbf{D} = \mathbf{H}_i = 0$. Defining with $\mathbf{K}_{ij}^{kl}$ the 2×2 matrix extracted by a generic 4×4 matrix $\mathbf{K}$ considering only the elements of rows i and j and columns k and l, putting $\bar{\mathbf{K}}_x = \mathbf{K}_{12}^{12} - \mathbf{K}_{12}^{34}(\mathbf{K}_{34\,xz}^{34})^{-1}\mathbf{K}_{34}^{12}$, $\bar{\mathbf{K}}_y = \mathbf{K}_{12}^{12} - \mathbf{K}_{12}^{34}(\mathbf{K}_{34\,yz}^{34})^{-1}\mathbf{K}_{34}^{12}$, $X_j = X_{j0}\exp(\mathrm{i}\Omega_n\theta/\Omega)$, $Y_j = -\mathrm{i}Y_{j0}\exp(\mathrm{i}\Omega_n\theta/\Omega)$, where the dimensionless precession speed $\Omega_n = \omega_n/\omega_c$ was introduced, the characteristic equation is a fourth degree algebraic equation in Ω_n^2, dependent on Ω^2

$$\begin{aligned} &\left[(\bar{K}_{x11} - \Omega_n^2)(\bar{K}_{x22} - J_d\Omega_n^2) - \bar{K}_{x12}^2\right] \\ &\quad \times \left[(\bar{K}_{y11} - \Omega_n^2)(\bar{K}_{y22} - J_d\Omega_n^2) - \bar{K}_{y12}^2\right] \\ &= (\bar{K}_{x11} - \Omega_n^2)(\bar{K}_{y11} - \Omega_n^2) J_a^2 \Omega^2 \Omega_n^2 \end{aligned} \tag{5}$$

The choice between the plus or minus sign for $\Omega_n = \pm\sqrt{\Omega_n^2}$ after solving Eq. (5) for Ω_n^2, may be done in view of getting equal signs for the amplitudes $X_{1,0}$ and $Y_{1,0}$, whence the whirling motion of the rotor centre is a progressive or retrograde precession for $\Omega_n > 0$ or $\Omega_n < 0$.

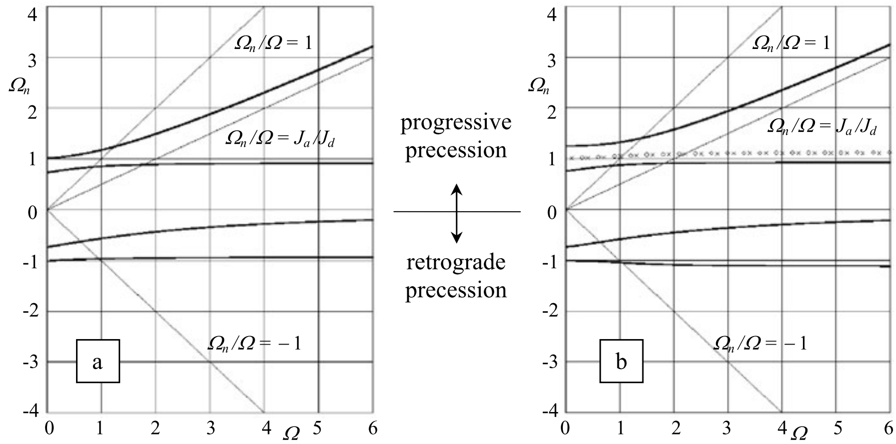

Fig. 2 Campbell diagrams $\Omega_n(\Omega)$ for $L_3 = 0.3$, $J_a = 0.1$, $J_d = 0.2$ (oblong inertia ellipsoid). (**a**): $K_{3x} = K_{4x} = 1$, $K_{3y} = K_{4y} = 1$, (**b**): $K_{3x} = K_{4x} = 1$, $K_{3y} = K_{4y} = 2$. *Circles*: axis whirl counter-directed. *Crosses*: front support whirl counter-directed

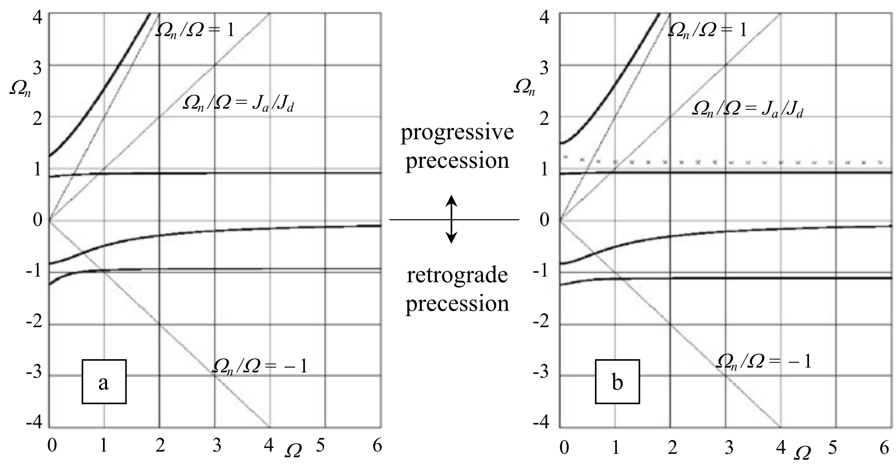

Fig. 3 Campbell diagrams $\Omega_n(\Omega)$ for $L_3 = 0.3$, $J_a = 0.2$, $J_d = 0.1$ (oblate inertia ellipsoid). (**a**): $K_{3x} = K_{4x} = 1$, $K_{3y} = K_{4y} = 1$, (**b**): $K_{3x} = K_{4x} = 1$, $K_{3y} = K_{4y} = 2$. *Crosses*: front support whirl counter-directed

Figures 2 and 3 show the Campbell diagrams for two examples cases, of an oblong and an oblate ellipsoid of inertia of the rotor. The left diagrams refer to isotropic support stiffness and the right ones to anisotropic stiffness. The continuous lines represent forward/backward whirl and refer to the motion of point O_1 and to the other motions with the same whirl direction. When on the contrary the whirl direction of one support or of the rotor axis is counter-directed with respect to the rotor centre, a plot with small circles or crosses is reported, symmetric of course of a continuous branch. Only equal-directed whirling motions may develop for isotropic support stiffness, whereas some whirling directions may be opposite to the rotor centre when the supports have quite different stiffness values on the two planes.

The response to unbalance can be detected applying a harmonic balance procedure after replacing $\mathbf{X} = \mathbf{X}_{c0}\cos\theta + \mathbf{X}_{s0}\sin\theta$, $\mathbf{Y} = \mathbf{Y}_{c0}\cos\theta + \mathbf{Y}_{s0}\sin\theta$ into Eqs. (3a) and (3b). A 16×16 algebraic system is obtained, whose solutions permits calculating the steady elliptical paths of the rotor and the supports.

The principal half-diameters and their angles with the fixed reference frame are:

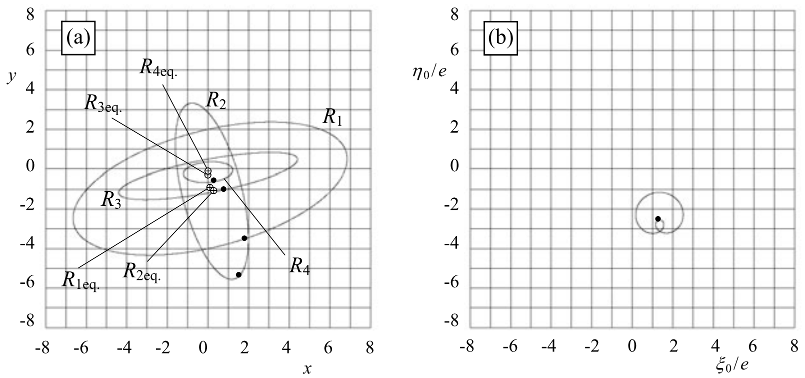

Fig. 4 (**a**) Elliptical path of point $O_1 (R_1 = r_1/e)$, of centres of back and front journal boxes ($R_3 = r_3/e$ and $R_4 = r_4/e$) and of rotor axis ($R_2 = l\sqrt{\varphi^2 + \psi^2}/e$), for $\Omega = 0.9$; (**b**) double looped path of point O_1 in the rotating frame $O_3\xi_0\eta_0\zeta_0$ for $\Omega = 0.9$. Data: $K_{3x} = K_{4x} = 1$, $K_{3y} = K_{4y} = 2$, $J_d = 0.1$, $J_a = 0.2$, $L_3 = 0.3$, $\Gamma = 1$, $M_d = 0.1$, $\gamma = 90°$, $d_1 = d_2 = 0.02$, $d_{3x} = d_{4x} = d_{3y} = d_{4y} = 0.1$, $d_{h1} = 0.1$, $d_{h2} = 0.05$

$$\begin{matrix} a_j \\ b_j \end{matrix} = \sqrt{\frac{Y_{c0,j}^2 + Y_{s0,j}^2 + X_{c0,j}^2 + X_{s0,j}^2 \pm \sqrt{(Y_{c0,j}^2 + Y_{s0,j}^2 - X_{c0,j}^2 - X_{s0,j}^2)^2 + 4(X_{c0j}Y_{c0j} + X_{s0j}Y_{s0j})^2}}{2}} \tag{6a}$$

$$\tan 2\phi_j = \frac{2(X_{c0j}Y_{c0j} + X_{s0j}Y_{s0j})}{X_{c0,j}^2 + X_{s0,j}^2 - Y_{c0,j}^2 - Y_{s0,j}^2} \tag{6b}$$

As an example, Fig. 4a shows the equilibrium points and the steady elliptical trajectories of the rotor and the supports during a complete wobbling cycle, for a particular under-critical case. Figure 4b shows the path of point O_1 in the rotating reference $O_3\xi_0\eta_0\zeta_0$, pointing out the double looped shape of the trajectory during one complete revolution.

The frequency response for the four whirling motions is also reported in Fig. 5 for an example case. The figures show the major and minor radii of the elliptical paths and the angle ϕ of the major axis with respect to the horizontal plane. It is observable that the rotor trajectory tends to a circle with radius equal to the mass eccentricity e for $\Omega \to \infty$, similarly to the conventional Laval-Jeffcott behavior: the centre of mass tends to its centred motionless position.

4 Stability of the steady motion

The motion stability can be inspected throughout the speed range by some perturbation approach, putting $\mathbf{X} = \mathbf{X}_{\mathrm{steady}} + \tilde{\mathbf{X}}$, $\mathbf{Y} = \mathbf{Y}_{\mathrm{steady}} + \tilde{\mathbf{Y}}$, where the subscript $\ldots_{\mathrm{steady}}$ indicates the previous steady solutions and the tilde refers to the small perturbations.

Assuming solutions of the type $\tilde{\mathbf{X}} = \tilde{\mathbf{X}}_0 \exp(\sigma\theta/\Omega)$, $\tilde{\mathbf{Y}} = \tilde{\mathbf{Y}}_0 \exp(\sigma\theta/\Omega)$, where σ is a characteristic number and using the previous notation, one gets the twelfth degree characteristic equation

$$\det\left(\begin{bmatrix} \mathbf{K}_{12}^{12} & \mathbf{K}_{12}^{34} & 0 & 0 \\ \mathbf{K}_{34}^{12} & \mathbf{K}_{34\,xz}^{34} & 0 & 0 \\ 0 & 0 & \mathbf{K}_{12}^{12} & \mathbf{K}_{12}^{34} \\ 0 & 0 & \mathbf{K}_{34}^{12} & \mathbf{K}_{34\,yz}^{34} \end{bmatrix} \right.$$

$$+ 2\sigma \begin{bmatrix} \mathbf{D}_{12}^{12} & 0 & 0 & 0 \\ 0 & \mathbf{D}_{34\,xz}^{34} & 0 & 0 \\ 0 & 0 & \mathbf{D}_{12}^{12} & 0 \\ 0 & 0 & 0 & \mathbf{D}_{34\,yz}^{34} \end{bmatrix}$$

$$+ 2\frac{\sigma}{\Omega} \begin{bmatrix} \mathbf{H}_{i,\,12}^{\ \ 12} & \mathbf{H}_{i,\,12}^{\ \ 34} & 0 & 0 \\ \mathbf{H}_{i,\,34}^{\ \ 12} & \mathbf{H}_{i,\,34}^{\ \ 34} & 0 & 0 \\ 0 & 0 & \mathbf{H}_{i,\,12}^{\ \ 12} & \mathbf{H}_{i,\,12}^{\ \ 34} \\ 0 & 0 & \mathbf{H}_{i,\,34}^{\ \ 12} & \mathbf{H}_{i,\,34}^{\ \ 34} \end{bmatrix}$$

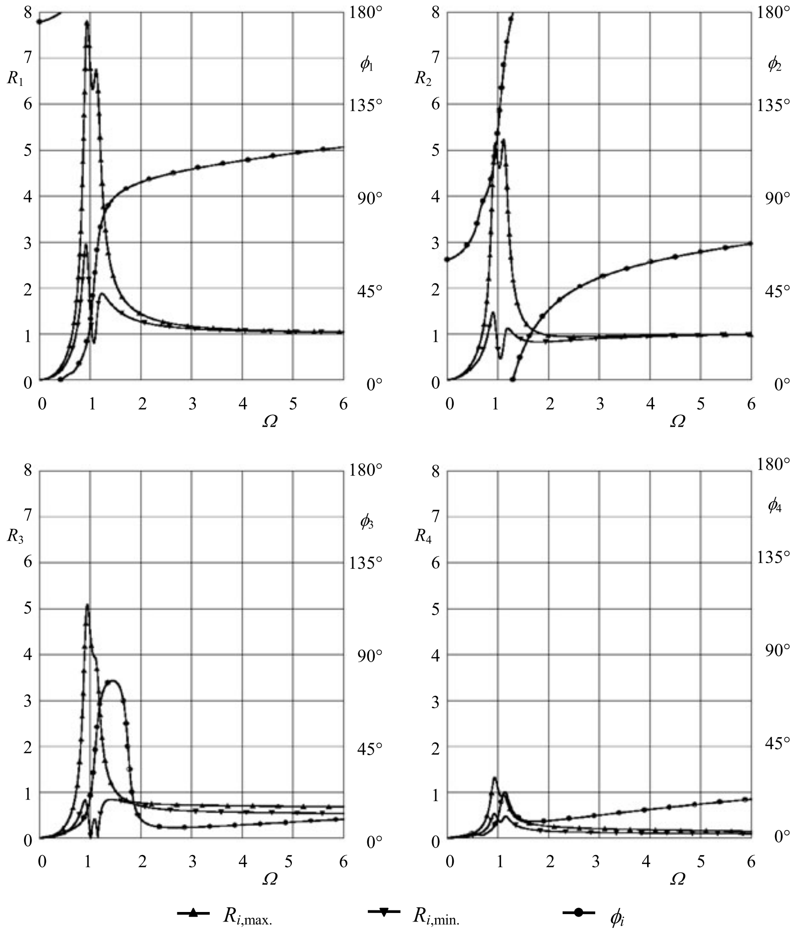

Fig. 5 Maximum and minimum orbital radii of the elliptical paths and slope of the principal axes vs rotor angular speed ($R_i = r_i/e$ for $i \neq 2$, $R_2 = l\sqrt{\varphi^2 + \psi^2}/e$). Data: $K_{3x} = K_{4x} = 1$, $K_{3y} = K_{4y} = 2$, $J_d = 0.1$, $J_a = 0.2$, $L_3 = 0.3$, $M_d = 0.1$, $\gamma = 90°$, $d_1 = d_2 = 0.02$, $d_{3x} = d_{4x} = d_{3y} = d_{4y} = 0.1$, $d_{h1} = 0.1$, $d_{h2} = 0.05$

$$+2\begin{bmatrix} 0 & 0 & \mathbf{H}_{i,12}^{\ 12} & \mathbf{H}_{i,12}^{\ 34} \\ 0 & 0 & \mathbf{H}_{i,34}^{\ 12} & \mathbf{H}_{i,34}^{\ 34} \\ -\mathbf{H}_{i,12}^{\ 12} & -\mathbf{H}_{i,12}^{\ 34} & 0 & 0 \\ -\mathbf{H}_{i,34}^{\ 12} & -\mathbf{H}_{i,34}^{\ 34} & 0 & 0 \end{bmatrix}$$

$$+\sigma^2\begin{bmatrix} \mathbf{M}_{12}^{12} & 0 & 0 & 0 \\ 0 & 0 & 0 & 0 \\ 0 & 0 & \mathbf{M}_{12}^{12} & 0 \\ 0 & 0 & 0 & 0 \end{bmatrix}$$

$$+\Omega\sigma\begin{bmatrix} 0 & 0 & \mathbf{G}_{12}^{12} & 0 \\ 0 & 0 & 0 & 0 \\ -\mathbf{G}_{12}^{12} & 0 & 0 & 0 \\ 0 & 0 & 0 & 0 \end{bmatrix}\Bigg) = 0 \qquad (7)$$

where the subscript i (= 1 or 2) of the hysteresis matrix has to be chosen in accordance with the prevailing of the gravity or the unbalance influence in the system under examination. The hysteretic factors are assumed for simplicity unaffected by the passage from the steady to the perturbed conditions. Equation (7) may be written in the compact form $E_c(\sigma) = b_0\sigma^{12} + b_1\sigma^{11} + \cdots + b_j\sigma^{12-j} + \cdots + b_{11}\sigma + b_{12} = 0$, where the coefficient b_0 of σ^{12} can be easily found to be equal to $16J_d^2[d_{3x}d_{4x} + d_{hi}(d_{3x}L_3^2 + d_{4x}L_4^2)/\Omega][d_{3y}d_{4y} + d_{hi}(d_{3y}L_3^2 + d_{4y}L_4^2)/\Omega] > 0$.

As regards the other coefficients, a collocation method may be applied, choosing six values σ_i arbitrarily for $i = 1, 2, \ldots, 6$, evaluating $E_c(\sigma_i)$ and $E_c(-\sigma_i)$ and composing two uncoupled 6×6 algebraic systems for the even and odd coefficients b_j:

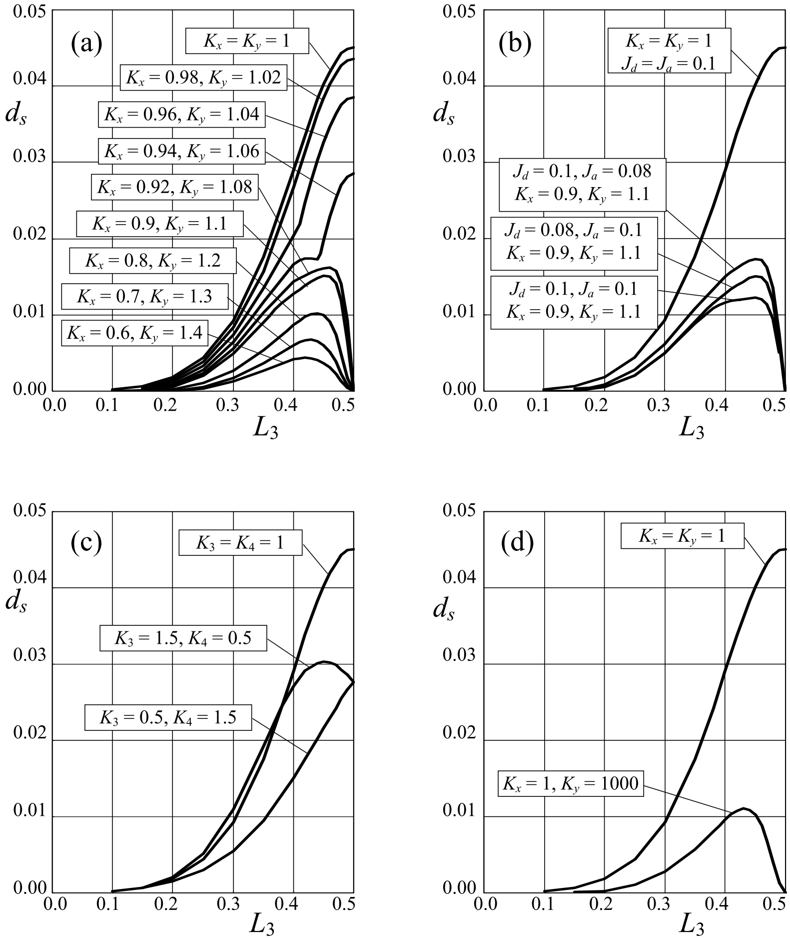

Fig. 6 Stability threshold d_s: $d_{3x} = d_{4x} = d_{3y} = d_{4y} = d_s$, $d_1 = d_2 = 0$, $d_{hi} = 0.02$. (**a**): Influence of support anisotropy ($J_d = 0.08$, $J_a = 0.1$, $K_{3x} = K_{4x} = K_x$, $K_{3y} = K_{4y} = K_y$); (**b**): gyro effect ($K_{3x} = K_{4x} = K_x$, $K_{3y} = K_{4y} = K_y$); (**c**): influence of support asymmetry ($J_d = 0.1$, $J_a = 0.1$, $K_{3x} = K_{3y} = K_3$, $K_{4x} = K_{4y} = K_4$); (**d**): comparison with "infinite" vertical stiffness ($J_d = 0.1$, $J_a = 0.1$, $K_{3x} = K_{4x} = K_x$, $K_{3y} = K_{4y} = K_y$)

$$\begin{aligned}
&\frac{E_c(\sigma_i) + E_c(-\sigma_i)}{2} - b_0\sigma_i^{12} \\
&\quad = b_2\sigma_i^{10} + b_4\sigma_i^8 + b_6\sigma_i^6 \\
&\qquad + b_8\sigma_i^4 + b_{10}\sigma_i^2 + b_{12} \\
&\frac{E_c(\sigma_i) - E_c(-\sigma_i)}{2} \\
&\quad = b_1\sigma_i^{11} + b_3\sigma_i^9 + b_5\sigma_i^7 \\
&\qquad + b_7\sigma_i^5 + b_9\sigma_i^3 + b_{11}\sigma_i
\end{aligned} \qquad (\text{for } i = 1 \text{ to } 6) \qquad (8)$$

Then, the usual Routh-Hurwitz procedure can be applied to calculate the thresholds of stability, i.e. the levels of the external viscous damping needed to nullify the destabilizing effect of the internal hysteresis. This is done exploring the speed range carefully for several values of the geometrical and mechanical parameters of the rotor-shaft-support system and increasing stepwise the external viscous damping by a trial and error technique. The main features of the system behavior are reported in the examples of Fig. 6, where the damping factors d_1 and d_2 are null and all the others are equal ($d_{3x} = d_{3y} = d_{4x} = d_{4y} = d_s$).

Figure 6a reports the stability threshold d_s as a function of the geometrical location of the rotor along the shaft and in particular shows the effect of the stiffness anisotropy of the supports. It is interesting that the increase in the stiffness anisotropy improves the stability of the whirling motion mainly if the rotor is mounted at the mid-span of the shaft. Actually, no external viscous dissipation source is required for symmetric systems if the relative difference between horizontal and vertical stiffness is larger than a certain limit value. This result agrees with the following section and with Ref. [9], but it is here shown how the beneficial influence of the support anisotropy decreases on shifting the rotor towards the one or the other support, unless the suspension system is isotropic, in which case the worst stability conditions are just found in the symmetric configuration.

Observe that, on increasing the difference $K_y - K_x$, the curves of Fig. 6a begin to show a sort of dip near $L_3 \cong 0.4$, which becomes more and more pronounced until turning the curve towards the point $L_3 = 0.5$, $d_s = 0$ for higher stiffness gaps (perfect stabilization). In this region however, the diagrams are quite steep, so that the best benefit of the suspension anisotropy appears confined to a rather narrow interval astraddle the mid-span, though it remains always favorable with respect to the pure isotropic case $K_y = K_x$ also for moderate values of $K_y - K_x$. Thus, the results of previous studies (e.g. [9]) are confirmed but appear strongly limited by an even small change of the rotor position in the neighborhood of the shaft middle section.

Figure 6b shows similar plots, but focuses on the gyro structure, which is found to exert a slight but clear destabilizing effect and in fact, the case of a spherical ellipsoid of inertia of the rotor ($J_a = J_d$) requires the lowest additional viscous damping to stabilize the rotor whirl.

The influence of the elastic dissymmetry between the front and back suspension is shown in Fig. 6c, whose diagrams may be prolonged for $L_3 > 0.5$ by mirror interchange of the two lower curves. These plots indicate the convenience of a more flexible suspension of the support closest to the rotor, particularly if the rotor is mounted roughly halfway between the mid-span and the support. On the other hand, it is to be observed that all diagrams of Figs. 6a, b, c, d indicate a stabilizing effect of the geometrical asymmetry of the rotor configuration and a negligible influence of the shaft hysteresis for $L_3 \to 0$.

At last, the case of"infinite" vertical stiffness (journal boxes moving only horizontally) is compared in Fig. 6d with the isotropic stiffness case: the unidirectional support compliance appears here much more convenient with respect to the axial-isotropic case.

The stability control can be carried out also by numerical integration, starting from random initial values and using some integration routine, for example of the Euler-Cauchy type, though this kind of approach is quite wearisome. Nevertheless, this turns out to be a convenient procedure when modelling the internal dissipation by the dry friction. Assuming this last friction model as the most appropriate for a particular system, the internal hysteretic force acting on the rotor has to be considered constant and opposite to the relative velocity with respect to the rotating frame shown in the detail of Fig. 1. Such a force has thus the two components $F_{hx} = -F_{h,\mathrm{dry}} v_{\mathrm{rel.},x} / \sqrt{v_{\mathrm{rel.},x}^2 + v_{\mathrm{rel.},y}^2}$, $F_{hy} = -F_{h,\mathrm{dry}} v_{\mathrm{rel.},y} / \sqrt{v_{\mathrm{rel.},x}^2 + v_{\mathrm{rel.},y}^2}$, where $v_{\mathrm{rel.},x} = \dot{x}_1 - \dot{x}_3 L_4 - \dot{x}_4 L_3 + \omega(y_1 - y_3 L_4 - y_4 L_3)$ and $v_{\mathrm{rel.},y} = \dot{y}_1 - \dot{y}_3 L_4 - \dot{y}_4 L_3 - \omega(x_1 - x_3 L_4 - x_4 L_3)$.

Observe that the differential system (3a), (3b) is of the twelfth order, as the support masses were neglected, and when integrating numerically, the third and fourth equations of (3a) and (3b) must be solved in advance for the four derivatives, X_3', X_4', Y_3', Y_4' at each step. This task can be fulfilled by simple inversion of sub-matrices in the viscous linear case, but must be carried out by some iterative procedure in the dry nonlinear one.

The numerical integration of Eqs. (3a) and (3b) permits comparing the results obtainable by the viscous and dry models. To this end, some equivalence criterion must be stated between the coefficients $F_{h,\mathrm{dry}}$ and c_h or else between the hysteresis factors $d_{h,\mathrm{dry}} = F_{h,\mathrm{dry}}/k_0 e$ and $d_h = 0.5 c_h \omega / k_0$, and this may be done for example by imposing the same dissipated work over a period of several revolutions of the rotor: $d_{h,\mathrm{dry}} = 2 d_h \int_\theta^{\theta+2N\pi} (\xi_0'^2 + \eta_0'^2) \mathrm{d}\theta / \int_\theta^{\theta+2N\pi} e \sqrt{\xi_0'^2 + \eta_0'^2} \mathrm{d}\theta$ where $N \gg 1$. During the calculation of the diagrams reported in the following Figs. 7 and 8, the dry coefficient $d_{h,\mathrm{dry}}$ was updated at the end of each long period according to this equivalence criterion, until it reached a nearly invariable asymptotic value. Then, the numerical integration re-started using this asymptotic value.

Figure 7 shows the transient path of point O_1, in the viscous and dry assumption, for a stable under-critical case. As clearly observable, the two diagrams exhibit nearly the same evolution and tend to the same elliptical path.

On the contrary, Fig. 8 refers to an unstable overcritical case, but shows that the two trajectories are

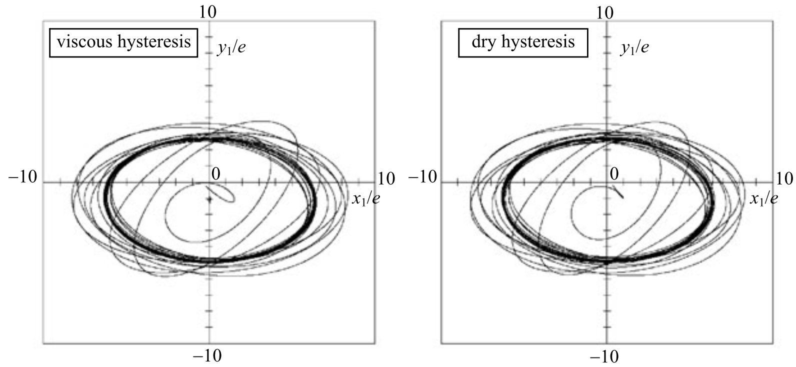

Fig. 7 Example of stable transient paths of point O_1, for viscous and dry hysteretic force and equal dissipative work (50 revolutions). Data: $K_{3x} = K_{3x} = 1$, $K_{3y} = K_{3y} = 3$, $J_d = 0.1$, $J_a = 0.2$, $L_3 = 0.4$, $\Gamma = 1$, $M_d = 1$, $\gamma = 90°$, $d_1 = d_2 = 0$, $d_{3x} = d_{4x} = d_{3y} = d_{4y} = 0.1$, $d_h = 0.02$, $d_{h,\mathrm{dry}} = 0.049$, $\Omega = 0.8$

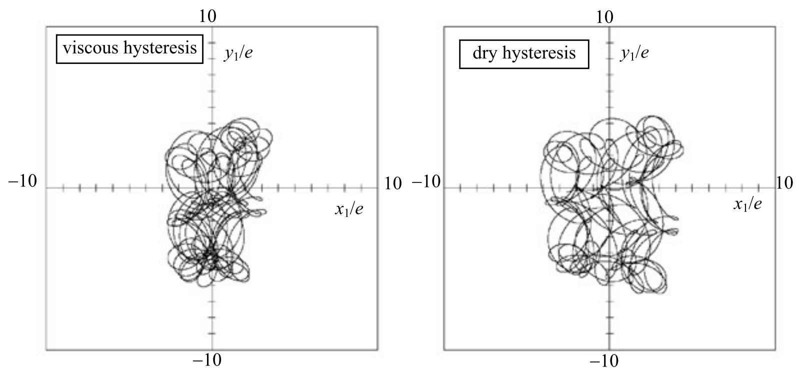

Fig. 8 Example of unstable transient paths of point O_1 for viscous and dry hysteretic force and equal dissipative work (50 revolutions). Data: $K_{3x} = K_{4x} = 1$, $K_{3y} = K_{4y} = 3$, $J_d = 0.1$, $J_a = 0.2$, $L_3 = 0.4$, $\Gamma = 1$, $M_d = 1$, $\gamma = 90°$, $d_1 = d_2 = 0$, $d_{3x} = d_{4x} = d_{3y} = d_{4y} = 0.005$, $d_h = 0.02$, $d_{h,\mathrm{dry}} = 0.012$, $\Omega = 5$

roughly similar. Moreover, checking several working conditions close to the stability threshold with slightly increasing external damping, it is observable that the threshold is reached a little in advance by the dry model. As a result the viscous hysteretic hypothesis appears conservative and can be conveniently applied also in the case of uncertainty about the amount of Coulombian friction within the whole internal dissipation.

5 The symmetric case

5.1 General approach

The effect of the stiffness anisotropy may be elucidated by the straightforward analysis of a rotor which is mounted at the shaft mid-span and is characterized by symmetric supports, $K_{3x} = K_{4x} = K_{x,tot.}/2$, $K_{3y} = K_{4y} = K_{y,tot.}/2$, equal damping factors of the supports, $d_{3x} = d_{4x} = d_{3y} = d_{4y} = d_{s,tot.}/2$, and zero external dissipative forces on the rotor, $d_1 = d_2 = 0$. In this case, the conical wobbling is uncoupled with the cylindrical whirling motion, independent of the hysteresis and stable. Putting $X_1 = X_r$, $X_3 + X_4 = 2X_s$, $Y_1 = Y_r$, $Y_3 + Y_4 = 2Y_s$, observing that $K_{jz11} = -2K_{jz13} = -2K_{jz14} = 1$, $2K_{jz33} = 2K_{jz44} = 1 + K_{j,tot.}$ (for $j = x$ or y), the perturbed cylindrical motions included in Eqs. (3a) and (3b) may be described by the simpler differential system:

$$X_r - X_s + 2d_{hi}\left(X_r' - X_s' + Y_r - Y_s\right) + \Omega^2 X_r'' = 0 \tag{9a}$$

$$-X_r+(1+K_{x,tot.})X_s+2\Omega d_{s,tot.}X_s' \\ -2d_{hi}\big(X_r'-X_s'+Y_r-Y_s\big)=0 \tag{9b}$$

$$Y_r-Y_s+2d_{hi}\big(Y_r'-Y_s'-X_r+X_s\big) \\ +\Omega^2 Y_r''=0 \tag{9c}$$

$$-Y_r+(1+K_{y,tot.})Y_s+2\Omega d_{s,tot.}Y_s' \\ -2d_{hi}\big(Y_r'-Y_s'-X_r+X_s\big)=0 \tag{9d}$$

where the tildes have been omitted.

Replacing solutions of the type $\exp(\sigma\theta/\Omega)$, it is easy to arrive at the sixth degree characteristic equation

$$\big(H^2+4d_{hi}^2\big)\big(A_x+\sigma^2\big)\big(A_y+\sigma^2\big)+\sigma^4 A_x A_y \\ +\sigma^2 H\big[A_x\big(A_y+\sigma^2\big)+A_y\big(A_x+\sigma^2\big)\big]=0 \tag{10}$$

where $H=1+2d_{hi}\sigma/\Omega$, $A_x=K_{x,tot.}+2d_{s,tot.}\sigma$, $A_y=K_{y,tot.}+2d_{s,tot.}\sigma$.

In the absence of hysteresis, Eq. (10) becomes $[\sigma^2(A_x+1)+A_x][\sigma^2(A_y+1)+A_y]=0$, whence the cubic equations result $2d_{s,tot.}\sigma^3+(1+K_{x,tot.\text{ or }y,tot.})\sigma^2+2d_{s,tot.}\sigma+K_{x,tot.\text{ or }y,tot.}=0$, whose roots have negative real parts by the Routh-Hurwitz criterion. In the presence of hysteresis, the coefficients $b_6,b_5,\dots,b_0$ of the characteristic polynomial are somewhat more complex and will be not reported here. However, it is observable that the fifth Routh-Hurwitz determinant RH_5 is the first one that becomes critical on increasing the hysteresis factor d_{hi}, while the other determinants remain positive. Neglecting the viscous damping, in order to assess the self-stabilizing aptitude of the system within pure ideal conditions, and assuming the very realistic hypothesis that $(2d_{hi}/\Omega)^2\ll 1$, this determinant may be ascertained as positive and then stable if the difference $(K_{y,tot.}-K_{x,tot.})$ is of the same order of magnitude of $K_{x,tot.}$ or $K_{y,tot.}$. When on the contrary $(K_{y,tot.}-K_{x,tot.})$ is of order d_{hi}, one can find $RH_5\cong(2+K_{x,tot.}+K_{y,tot.})(K_{x,tot.}K_{y,tot.})^2(2d_{hi}/\Omega)^3\{(K_{y,tot.}-K_{x,tot.})^2-8d_{hi}^2[(K_{y,tot.}-K_{x,tot.})^2+2(K_{x,tot.}K_{y,tot.})^2]\}$ as the dominant part of RH_5, whence the following stability limit may be obtained irrespective of the angular speed

$$\left|\frac{K_{x,tot.}K_{y,tot.}}{K_{y,tot.}-K_{x,tot.}}\right|<\sqrt{\frac{1}{16d_{hi}^2}-\frac{1}{2}}\cong\frac{1}{4d_{hi}} \tag{11}$$

This result is in perfect accordance with Fig. 6a, b for $L_3=1/2$ and points out how the elastic anisotropy of the supports may exert a strong stabilizing effect.

5.2 Small perturbation approach

Another different approach leads to concordant results, but clarifies better the stabilizing aptitude of the stiffness anisotropy of the suspension.

Putting $\mathbf{U}=\mathbf{X}+\mathrm{i}\mathbf{Y}$, $\mathbf{V}=\mathbf{X}-\mathrm{i}\mathbf{Y}$, multiplying Eqs. (9c) and (9d) by the imaginary unit i, summing and subtracting them from Eqs. (9a) and (9b) respectively, one gets

$$U_r-U_s+2d_{hi}\big[\big(U_r'-U_s'\big)-\mathrm{i}(U_r-U_s)\big] \\ +\Omega^2 U_r''=0 \tag{12a}$$

$$-U_r+\left(1+\frac{K_{x,tot.}+K_{y,tot.}}{2}\right)U_s \\ +\frac{K_{x,tot.}-K_{y,tot.}}{2}V_s+2\Omega d_{s,tot.}U_s' \\ -2d_{hi}\big[\big(U_r'-U_s'\big)-\mathrm{i}(U_r-U_s)\big]=0 \tag{12b}$$

$$V_r-V_s+2d_{hi}\big[\big(V_r'-V_s'\big)+\mathrm{i}(V_r-V_s)\big] \\ +\Omega^2 V_r''=0 \tag{12c}$$

$$-V_r+\left(1+\frac{K_{x,tot.}+K_{y,tot.}}{2}\right)V_s \\ +\frac{K_{x,tot.}-K_{y,tot.}}{2}U_s+2\Omega d_{s,tot.}V_s' \\ -2d_{hi}\big[\big(V_r'+V_s'\big)+\mathrm{i}(V_r-V_s)\big]=0 \tag{12d}$$

In the hypothesis that the dissipative factors d_s and d_{hi} are small, the characteristics roots of systems (9a)–(9d) and (12d)–(12d) are very close to the natural frequencies Ω_n. Therefore, putting $\mathbf{U}=\mathbf{U}_0\exp(\mathrm{i}\sigma\theta/\Omega)$, $\mathbf{V}=\mathbf{V}_0\exp(\mathrm{i}\sigma\theta/\Omega)$, where σ is nearly real and very close to one of the Ω_n's and the constant vectors $\mathbf{U}_0$ and $\mathbf{V}_0$ are nearly real as well, it is easy to recognize that $\mathbf{U}$ and $\mathbf{V}$ describe progressive and retrograde precession motions respectively for $\mathrm{Real}(\sigma)>0$, or vice versa for $\mathrm{Real}(\sigma)<0$, which motions are coupled with each other through the differential stiffness coefficient $(K_{x,tot.}-K_{y,tot.})/2$. In accordance with the elliptic shape of the orbital paths, all natural modes turn out to be composed of progressive and retrograde circular motions, which become uncoupled for $K_{x,tot.}=K_{y,tot.}$. Notice that the ideal non-dissipative natural modes are uncoupled in the horizontal and vertical planes by Eqs. (9a)–(9d).

All small parameters can be scaled by d_{hi}, putting $d_{s,tot.}=\delta d_{hi}$ and $\sigma=\Omega_n+\mathrm{i}\lambda d_{hi}$, where δ and λ are numbers of order one. Then, replacing the above exponential solutions into Eqs. (12a)–(12d) and retaining only the terms of order 1 and d_{hi}, one gets a complex algebraic system for U_{r0}, U_{s0}, V_{r0}, V_{s0}, whose coefficients are given by the matrix

$$\begin{bmatrix} 1-\Omega_n^2+2\mathrm{i}d_{hi}(s^{(-)}-\lambda\Omega_n) & -1-2\mathrm{i}d_{hi}s^{(-)} & 0 & 0 \\ -1-2\mathrm{i}d_{hi}s^{(-)} & 1+\frac{K_{x,tot.}+K_{y,tot.}}{2}+2\mathrm{i}d_{hi}(s^{(-)}+\delta\Omega_n) & 0 & \frac{K_{x,tot.}-K_{y,tot.}}{2} \\ 0 & 0 & 1-\Omega_n^2+2\mathrm{i}d_{hi}(s^{(+)}-\lambda\Omega_n) & -1-2\mathrm{i}d_{hi}s^{(+)} \\ 0 & \frac{K_{x,tot.}-K_{y,tot.}}{2} & -1-2\mathrm{i}d_{hi}s^{(+)} & 1+\frac{K_{x,tot.}+K_{y,tot.}}{2}+2\mathrm{i}d_{hi}(s^{(+)}+\delta\Omega_n) \end{bmatrix} \tag{13}$$

where one has put $s^{(-)}=\Omega_n/\Omega-1$ and $s^{(+)}=\Omega_n/\Omega+1$.

Cancelling the terms containing $2\mathrm{i}d_{hi}$, we get the ideal natural frequencies through the characteristic equation:

$$\left[\left(1+\frac{K_{x,tot.}+K_{y,tot.}}{2}\right)(1-\Omega_n^2)-1\right]^2 - \left(\frac{K_{x,tot.}-K_{y,tot.}}{2}\right)^2(1-\Omega_n^2)^2=0 \tag{14}$$

whence $\Omega_n^2=1/(1+1/K_{x,tot.\text{ or }y,tot.})$ for $d_{s,tot.}=d_{hi}=0$, as also calculable by Eqs. (9a)–(9d).

The first order correction λ to the eigenvalues of system (12a)–(12d) may be obtained multiplying the terms with $2\mathrm{i}d_{h1}$ in the determinant of (13) by their cofactors in the ideal matrix with $d_{hi}=0$. After some algebra, one gets

$$2\mathrm{i}d_{hi}\left[\left(1+\frac{K_{x,tot.}+K_{y,tot.}}{2}\right)(1-\Omega_n^2)-1\right] \times\left(\frac{\Omega_n}{1-\Omega_n^2}\right)\left[(s^{(-)}+s^{(+)})\Omega_n^3 + 2\delta(1-\Omega_n^2)^2-2\lambda\right]=0 \tag{15}$$

Since the quantity $(s^{(-)}+s^{(+)})\Omega_n^3=2\Omega_n^4/\Omega$ is always positive, Eqs. (14) and (15) clearly indicate that λ is real and positive, so that the motion appears stable. Nevertheless, for small anisotropy, i.e. for $(K_{x,tot.}-K_{y,tot.})/2$ of the same order of d_{hi}, the left hand of Eq. (15) becomes of order d_{hi}^2 by Eq. (14) and Eq. (15) does no longer hold true in a first approximation analysis, as other terms should be taken into account in the development of the determinant (13): the results from Eq. (15) are then valid only for relatively large anisotropy and reveal stability, in accordance with the previous approach.

For $(K_{x,tot.}-K_{y,tot.})/2$ of order d_{hi}, one can put $K_m=(K_{x,tot.}+K_{y,tot.})/2$, $\kappa d_{hi}=(K_{x,tot.}-K_{y,tot.})/2$, $K_{x,tot.}=K_m+\kappa d_{hi}$, $K_{y,tot.}=K_m-\kappa d_{hi}$, where $\kappa=O(1)$, and the characteristic equation (14) becomes $[(1+K_m)(1-\Omega_n^2)-1]^2=0$ (for $d_{hi}\to 0$), whence $\Omega_n^2=K_m/(1+K_m)$ twice. The dominant terms of the complete characteristic equation lead to

$$\frac{4d_{hi}^2}{(1+K_m)^2}\left\{\left[s^{(-)}K_m^2+\delta\Omega_n-\lambda\Omega_n(1+K_m)^2\right] \times\left[s^{(+)}K_m^2+\delta\Omega_n-\lambda\Omega_n(1+K_m)^2\right]+\frac{\kappa^2}{4}\right\}=0 \tag{16}$$

and, as $s^{(\pm)}=\Omega_n/\Omega\pm 1$ and $\Omega_n=\pm\sqrt{K_m/(1+K_m)}$, Eq. (16) gives

$$\left[\frac{K_m^2}{\Omega}+\delta-\lambda(1+K_m)^2\right]^2\left(\frac{K_m}{1+K_m}\right) - K_m^4+\frac{\kappa^2}{4}=0 \quad\to$$

$$\frac{K_m^2}{\Omega}+\delta-\lambda(1+K_m)^2 =\pm\sqrt{\left(\frac{1+K_m}{K_m}\right)\left(K_m^4-\frac{\kappa^2}{4}\right)} \tag{17}$$

Equation (17) points out that the absolute stability (for $0<\Omega<\infty$) can be obtained only for

$\delta^2 > (1+1/K_m)(K_m^4 - \kappa^2/4)$ if $K_m^4 > \kappa^2/4$. The stability is always ensured for any viscous level δ on the contrary, even for $\delta \to 0$, if $K_m^4 < \kappa^2/4$, which condition is exactly equal to Eq. (11), if one minds that $K_{x,tot.} K_{y,tot.} = K_m^2 + O(d_{hi})$ and $\kappa^2/4 = [(K_{x,tot.} - K_{y,tot.})/(4d_{hi})]^2$.

As the perturbed motions under examination are very close to the natural precession motions, it is also possible to opt for a slightly greater precision in the definition of the hysteretic effect and consider such motions affected by their own hysteretic coefficients $c_{hn} = h/|\omega_n - \omega|$, inversely proportional to the relative angular speed $|\omega_n - \omega|$ [31]. Therefore, recalling that one has $c_{h1} = h/\omega$ and $d_{h1} = 0.5h/k_0$ for the relative rotation of the equilibrium deflection plane, the hysteretic damping factors d_{hi} of Eqs. (12a)–(12d) could be replaced by the more specific ones $d_{hn} = c_{hn}\omega/2k_0 = (c_{hn}/c_{h1})h/2k_0 = d_{h1}/|\Omega_n/\Omega - 1|$. After these corrections, the quantities $s^{(\pm)}$ would now stand for $\operatorname{sgn}(\Omega_n/\Omega \pm 1)$ in Eq. (16) and one would have $s^{(+)} = 1$, $s^{(-)} = -1$ in the supercritical regime. As a consequence, Eq. (17) would still be applicable, save the disappearance of the term K_m^2/Ω, and the final result (11) would then remain unchanged.

5.3 Averaging technique

A new original approach, which may be considered as an extension of the Krylov-Bogoliubov method [32] to several degrees of freedom, can be also applied to the search of the stability threshold for weakly non-linear systems. This procedure is well suited for autonomous systems and is here applied in the hypothesis of absence of gravity and unbalance, in order to confirm the equivalence between dry and viscous internal dissipation.

Summing Eqs. (9a) and (9b), summing Eqs. (9c) and (9d), indicating the small parameter d_{hi} with ε and using the previous notation for the other quantities, one gets

$$\Omega^2 X_r'' + K_m X_s + \varepsilon\big(2\Omega\delta X_s' + \kappa X_s\big) = 0 \tag{18a}$$

$$\Omega^2 X_r'' + X_r - X_s + \varepsilon\Phi_X = 0 \tag{18b}$$

$$\Omega^2 Y_r'' + K_m Y_s + \varepsilon\big(2\Omega\delta Y_s' - \kappa Y_s\big) = 0 \tag{18c}$$

$$\Omega^2 Y_r'' + Y_r - Y_s + \varepsilon\Phi_Y = 0 \tag{18d}$$

where one has to put $\Phi_X = (d_{h,\mathrm{dry}}/d_{hi})\cos\psi$ and $\Phi_Y = (d_{h,\mathrm{dry}}/d_{hi})\sin\psi$ for non-linear dry friction, where $\tan\psi = (Y_r' - Y_s' - X_r + X_s)/(X_r' - X_s' + Y_r - Y_s)$, while $\Phi_X = 2(X_r' - X_s' + Y_r - Y_s)$ and $\Phi_Y = 2(Y_r' - Y_s' - X_r + X_s)$ for viscous friction.

The zero order solution ($\varepsilon = 0$) is $X_r = A\cos(\rho\theta + \alpha)$, $Y_r = B\sin(\rho\theta + \beta)$, $X_s = \Omega_n^2 X_r/K_m$, $Y_s = \Omega_n^2 Y_r/K_m$, where $\rho = \Omega_n/\Omega$, $\Omega_n^2 = K_m/(1+K_m)$. Hence, similarly to the Krylov-Bogoliubov procedure, one can try a first order solution of the type $X_r = A(\theta)\cos[\rho\theta + \alpha(\theta)]$, $Y_r = B(\theta)\sin[\rho\theta + \beta(\theta)]$, $X_s = \Omega_n^2 X_r/K_m + a(\theta)$, $Y_s = \Omega_n^2 Y_r/K_m + b(\theta)$, and impose the extra conditions $X_r' = -\rho A(\theta)\sin[\rho\theta + \alpha(\theta)]$, $Y_r' = \rho B(\theta)\cos[\rho\theta + \beta(\theta)]$. Replacing this solution into Eqs. (18a)–(18d) and neglecting terms of order ε^2 or smaller, one obtains two coupled differential systems for the six unknown functions $A(\theta)$, $B(\theta)$, $\alpha(\theta)$, $\beta(\theta)$, $a(\theta)$, $b(\theta)$:

$$A\alpha'\Omega_n\Omega\cos(\tau-\mu) + A'\Omega_n\Omega\sin(\tau-\mu) - K_m a = \varepsilon\frac{\Omega_n^2}{K_m}A\big[\kappa\cos(\tau-\mu) - 2\delta\Omega_n\sin(\tau-\mu)\big] \tag{19a}$$

$$A\alpha'\Omega_n\Omega\cos(\tau-\mu) + A'\Omega_n\Omega\sin(\tau-\mu) + a = \varepsilon\Phi_X \tag{19b}$$

$$A\alpha'\sin(\tau-\mu) - A'\cos(\tau-\mu) = 0 \tag{19c}$$

$$B\beta'\Omega_n\Omega\sin(\tau+\mu) - B'\Omega_n\Omega\cos(\tau+\mu) - K_m b = \varepsilon\frac{\Omega_n^2}{K_m}B\big[2\delta\Omega_n\cos(\tau+\mu) - \kappa\sin(\tau+\mu)\big] \tag{20a}$$

$$B\beta'\Omega_n\Omega\sin(\tau+\mu) - B'\Omega_n\Omega\cos(\tau+\mu) + b = \varepsilon\Phi_Y \tag{20b}$$

$$B\beta'\cos(\tau+\mu) + B'\sin(\tau+\mu) = 0 \tag{20c}$$

where it was put $\tau = \rho\theta + (\alpha+\beta)/2$ and $\mu = (\beta-\alpha)/2$ for brevity. Equations (19a)–(19c) and (20a)–(20c) indicate that the quantities A', α', a, B', β' and b are small of order ε, whence the amplitudes $A(\theta)$ and $B(\theta)$ and the phases $\alpha(\theta)$ and $\beta(\theta)$ vary much more slowly than the argument $\rho\theta$.

Considering only the dominant terms of Φ_X and Φ_Y and carrying out some calculations, we may arrive at

$$\Phi_X = \left(\frac{d_{h,\mathrm{dry}}}{d_{hi}}\right)\frac{B\sin(\tau+\mu) - A\rho\sin(\tau-\mu)}{\sqrt{W}\sqrt{1-k^2\sin^2(\tau-\phi)}} \tag{21a}$$

$$\Phi_Y = \left(\frac{d_{h,\mathrm{dry}}}{d_{hi}}\right)\frac{\rho B\cos(\tau+\mu) - A\cos(\tau-\mu)}{\sqrt{W}\sqrt{1-k^2\sin^2(\tau-\phi)}} \tag{21b}$$

where $\tan 2\phi = [(A^2+B^2)/(A^2-B^2)]\tan 2\mu$ and

$$W = \frac{(A^2+B^2)(1+\rho^2) - 4AB\rho\cos 2\mu + |1-\rho^2|\sqrt{A^4+B^4-2A^2B^2\cos 4\mu}}{2} \tag{22a}$$

$$k^2 = \frac{2|1-\rho^2|\sqrt{A^4+B^4-2A^2B^2\cos 4\mu}}{(A^2+B^2)(1+\rho^2) - 4AB\rho\cos 2\mu + |1-\rho^2|\sqrt{A^4+B^4-2A^2B^2\cos 4\mu}} \tag{22b}$$

Moreover, neglecting the change of the slowly varying variables, the condition of equal dissipative work for dry and viscous friction reads

$$\begin{aligned}\frac{d_{h,\mathrm{dry}}}{d_{hi}} &= 2\Omega_n^2\sqrt{W}\left\{\frac{\int_0^{2\pi}[1-k^2\sin^2(\tau-\phi)]\mathrm{d}\theta}{\int_0^{2\pi}\sqrt{1-k^2\sin^2(\tau-\phi)}\mathrm{d}\theta}\right\} \\ &= \frac{\pi\Omega_n^2\sqrt{W}(1-\frac{k^2}{2})}{E(k)}\end{aligned} \tag{23}$$

where $E(k)$ is the Legendre's complete elliptic integral of the second kind.

Replacing Eqs. (21a) and (21b) into Eqs. (19a)–(19c) and (20a)–(20c), using Eqs. (22a), (22b) and (23), solving for A', B', α', β', and integrating with respect to the "quick" variable τ over a period 2π, the gradients A', α', B', β' turn out to be functions of the complete elliptic integrals of the first and second kinds, whose values may be found tabulated in several mathematical handbooks. Putting $\varepsilon_\Omega = \varepsilon/[\Omega\Omega_n(1+K_m)^2]$, one gets

$$\begin{aligned}A' = \varepsilon_\Omega\Bigg(K_m^2\bigg\{&\frac{(2-k^2)[K(k)-E(k)]}{k^2E(k)} \\ &\times\left[B\cos 2\phi - \rho A\cos 2(\mu-\phi)\right] \\ &- \frac{(2-k^2)K(k)}{2E(k)}\big[B(\cos 2\phi - \cos 2\mu) \\ &+ \rho A - \rho A\cos 2(\mu-\phi)\big]\bigg\} - \delta\Omega_n A\Bigg)\end{aligned} \tag{24a}$$

$$\begin{aligned}B' = \varepsilon_\Omega\Bigg(-K_m^2\bigg\{&\frac{(2-k^2)[K(k)-E(k)]}{k^2E(k)} \\ &\times\left[A\cos 2\phi - \rho B\cos 2(\mu+\phi)\right] \\ &+ \frac{(2-k^2)K(k)}{2E(k)}\big[-A(\cos 2\mu + \cos 2\phi) \\ &+ \rho B + \rho B\cos 2(\mu+\phi)\big]\bigg\} - \delta\Omega_n B\Bigg)\end{aligned} \tag{24b}$$

$$\begin{aligned}A\alpha' = \varepsilon_\Omega\Bigg(K_m^2\bigg\{&-\frac{(2-k^2)[K(k)-E(k)]}{k^2E(k)} \\ &\times\left[B\sin 2\phi + \rho A\sin 2(\mu-\phi)\right] \\ &+ \frac{(2-k^2)K(k)}{2E(k)}\big[B(\sin 2\mu + \sin 2\phi) \\ &+ \rho A\sin 2(\mu-\phi)\big]\bigg\} + \frac{\kappa}{2}A\Bigg)\end{aligned} \tag{24c}$$

$$\begin{aligned}B\beta' = \varepsilon_\Omega\Bigg(K_m^2\bigg\{&\frac{(2-k^2)[K(k)-E(k)]}{k^2E(k)} \\ &\times\left[A\sin 2\phi - \rho B\sin 2(\mu+\phi)\right] \\ &- \frac{(2-k^2)K(k)}{2E(k)}\big[A(\sin 2\mu + \sin 2\phi) \\ &- \rho B\sin 2(\mu+\phi)\big]\bigg\} - \frac{\kappa}{2}B\Bigg)\end{aligned} \tag{24d}$$

where $K(k)$ is the Legendre complete elliptic integral of the first kind.

The problem is thus formally solved and, though it is still non-linear and somewhat difficult in appearance, may lead to a simple stability analysis. Actually, both the quantities $(2-k^2)[K(k)-E(k)]/[k^2E(k)]$ and $(2-k^2)K(k)/[2E(k)]$, appearing in Eqs. (24a)–(24d), tend to the unity for $k \to 0$, i.e. on approaching the critical speed $\rho \cong 1$ (22b) and increase just slightly on increasing k, but keeping very close to one as long as $k < 0.8$ roughly. Then, simple approximate results are obtainable letting $k \to 0$, $E(k) \to \pi/2$, $K(k) \to \pi/2$ and $K(k) - E(k) \to \pi k^2/4$:

$$A' = \varepsilon_\Omega\left[K_m^2 B\cos 2\mu - \Omega_n\left(\delta + \frac{K_m^2}{\Omega}\right)A\right] \tag{25a}$$

$$B' = \varepsilon_\Omega\left[K_m^2 A\cos 2\mu - \Omega_n\left(\delta + \frac{K_m^2}{\Omega}\right)B\right] \tag{25b}$$

$$A\alpha' = \varepsilon_\Omega\left(K_m^2 B\sin 2\mu + \frac{\kappa}{2}A\right) \tag{25c}$$

$$B\beta' = -\varepsilon_\Omega\left(K_m^2 A\sin 2\mu + \frac{\kappa}{2}B\right) \tag{25d}$$

Multiplying Eq. (25a) by A, Eq. (25b) by B and subtracting, one obtains $(A^2-B^2)' = -2\varepsilon_\Omega\Omega_n(\delta + K_m^2/\Omega)(A^2-B^2)$, whence $A - B \to 0$ and we may put $A \cong R$, $B \cong R$ after some time. Hence, Eqs. (25a), (25b) become

$$\frac{R'}{R} = \varepsilon_\Omega \left[K_m^2 \cos 2\mu - \Omega_n \left(\delta + \frac{K_m^2}{\Omega} \right) \right] \tag{26}$$

while Eqs. (25c), (25d) give

$$\mu' = -\varepsilon_\Omega \left(K_m^2 \sin 2\mu + \frac{\kappa}{2} \right) \tag{27}$$

This last equation can be integrated, giving

$$\tan\mu = \sqrt{1 - \frac{4K_m^4}{\kappa^2}} \tan\left(-\varepsilon_\Omega \vartheta \sqrt{\frac{\kappa^2}{4} - K_m^4} \right) - \frac{2K_m^2}{\kappa} \quad \text{for } \kappa^2 > 4K_m^4 \tag{28a}$$

$$\tan\mu = \frac{(\frac{2K_m^2}{\kappa} + \sqrt{\frac{4K_m^4}{\kappa^2} - 1}) \exp(-2\varepsilon_\Omega \vartheta \sqrt{K_m^4 - \frac{\kappa^2}{4}}) - (\frac{2K_m^2}{\kappa} - \sqrt{\frac{4K_m^4}{\kappa^2} - 1})}{1 - \exp(-2\varepsilon_\Omega \vartheta \sqrt{K_m^4 - \frac{\kappa^2}{4}})} \quad \text{for } \kappa^2 < 4K_m^4 \tag{28b}$$

where the new variable $\vartheta = \theta - \theta_0$ includes the integration constant θ_0.

Equations (28a), (28b) permit expressing $\cos 2\mu$ as a function of ϑ and integrating Eq. (26). Omitting the calculation procedure for brevity, it is possible to find that $\int_0^\vartheta [K_m^2 \cos 2\mu - \Omega_n(\delta + K_m^2/\Omega)]\mathrm{d}\vartheta$ is a diverging negative function of ϑ for $\kappa^2 > 4K_m^4$, whereas it is easily observable that $\tan\mu \to \sqrt{4K_m^4/\kappa^2 - 1} - 2K_m^2/\kappa$ for $\vartheta \to \infty$ when $\kappa^2 < 4K_m^4$, implying that μ tends to an asymptotic nonzero value and $\sin 2\mu \to -\kappa/2K_m^2$. Therefore, R tends to vanish and the motion is certainly stable for $\kappa^2 > 4K_m^4$, as also ascertained through Eq. (17) by the previous approach, whereas for $\kappa^2 < 4K_m^2$, replacing $\cos 2\mu = \pm\sqrt{1 - (\kappa/2K_m^2)^2}$ into Eq. (26), it is possible to arrive at the stability condition $\pm\sqrt{K_m^4 - \kappa^2/4} < \Omega_n(\delta + K_m^2/\Omega)$, which is exactly the same as Eq. (17). Thus, using the averaging approach, we obtain similar results for linear and nonlinear internal friction.

Clearly the treatment of cases with a larger modulus k is more wearisome and the numerical solution of Eqs. (18a)–(18d) turns out to be preferable, though it is still possible to face the problem by simple approximation formulas for the elliptic integrals [33]. Anyway, also the above procedure confirms the result similarity of the viscous and dry models for the internal friction, provided that the equivalence of the dissipative work per cycle is properly imposed.

5.4 Concluding remarks on progressive and retrograde motions

Should we consider the true isotropic case $K_{x,tot.} = K_{y,tot.} = K_m$, $\kappa = 0$, Eqs. (12a) and (12b) would be uncoupled with Eqs. (12c) and (12d), the ideal natural frequencies would be given by $\Omega_n^2 = K_m/(1 + K_m)$ (twice) and the stability equation (16) would change into $s^{(\pm)} K_m \sqrt{K_m(1 + K_m)} + \delta - \lambda(1 + K_m)^2 = 0$, the minus and plus signs referring to progressive and retrograde rotations respectively (**U** progressive and **V** retrograde for $\Omega_n > 0$). While the retrograde motions **V** are stable, the progressive ones **U** may happen to become unstable on increasing the angular speed, as $s^{(-)}$ becomes negative. Nonetheless, the condition of absolute stability ($\lambda > 0$ for $\omega \to \infty$) would still be $\delta - K_m\sqrt{K_m(1 + K_m)} > 0$ and it is also remarkable that all the above results are valid for both the hypotheses, that $s^{(\pm)} = \Omega_n/\Omega \pm 1$, or else that $s^{(\pm)} = \mathrm{sgn}(\Omega_n/\Omega \pm 1)$. The same results are obtainable for the non-linear case by the previous averaging approach. For $\kappa = 0$ in fact, Eq. (27) indicates that $\mu \to 0$, whence Eq. (26) yields the stability condition $K_m^4 < \Omega_n^2(\delta + K_m^2/\Omega)^2$.

Summing up, Eq. (16) yields the interesting indication that the stabilizing effect of the stiffness anisotropy of the supports is associated in practice to a sort of coupling between progressive and retrograde precession motions ($\kappa \neq 0$), which coupling is absent in the isotropic systems ($\kappa = 0$).

6 Conclusion

The present paper discusses how to counteract the destabilizing effect of the shaft internal hysteresis in the supercritical regime of a rotating machine by making use of other dissipative sources or by planning anisotropic support stiffness, differentiated in the horizontal and vertical planes. An equivalent coefficient of linear viscous damping, inversely proportional to the angular speed, may be introduced for the calculation of the hysteretic friction force, which may be assumed proportional to the rotor centre velocity relative to a reference frame rotating with the shaft end sections. Otherwise, in the hypothesis of Coulombian internal friction, the internal force may be assumed as constant and constantly in opposition to the relative velocity. The natural precession modes and frequencies are easily calculated, and assuming some small unbalance, the elliptical paths of the rotor and the bearings, together with the conical locus of the rotor axis, are inspected throughout the speed range. The Routh-Hurwitz procedure may be applied to control the stability of the steady motion and the influence of several design characteristics of the rotor system on the stability may be analyzed, searching in particular for the viscous level needed for the stabilization in the whole speed range. The results confirm that the rotor whirl instability may be conveniently counterbalanced by planning different suspension stiffness characteristics in the horizontal and vertical planes, or in general in two orthogonal planes through the bearing centres. Nevertheless, this favorable effect is remarkable for rotors equidistant from the supports, but tends to become much less efficacious when the rotor is mounted away from the mid-span. A first approximation analytical approach points out that this stabilizing effect may be thought as associated with the coupling between progressive and retrograde precession motions. The two different hypotheses about the internal friction, viscous or dry, do not affect remarkably the response and the stability of the rotating system, provided that the comparison is made in conditions of equal dissipative work per shaft revolution.

References

1. Montagnier O, Hochard Ch (2007) Dynamic instability of supercritical drive shafts mounted on dissipative supports—effects of viscous and hysteretic internal damping. J Sound Vib 305(3):378–400
2. Sorge F (2008) Rotor whirl damping by dry friction suspension systems. Meccanica 43(6):577–589
3. Sorge F (2009) Damping of rotor conical whirl by asymmetric dry friction suspension. J Sound Vib 321(1–2):79–103
4. Sorge F, Cammalleri M (2009) Hysteretic whirl stabilization in rotor-shaft-bearing systems on dry friction suspension. In: XIX AIMETA national congress, Ancona, Italy, 14–17 September, cd-rom
5. Sorge F, Cammalleri M (2010) Control of hysteretic instability in rotating machinery by elastic suspension systems subject to dry and viscous friction. J Sound Vib 329(1–2):1686–1701
6. Newkirk BL (1924) Shaft whipping. General Electric Review 27:169–178
7. Kimball AL (1924) Internal friction theory of shaft whirling. General Electric Review 27:244–251
8. Robertson D (1935) Hysteretic influences on the whirling of rotors. Proc Inst Mech Eng 131:513–537
9. Gunter EJ Jr, Trumpler PR (1969) The influence of internal friction on the stability of high speed rotors with anisotropic supports. ASME J Eng Ind 91:1105–1113
10. Chang CO, Cheng JW (1993) Non-linear dynamics and instability of a rotating shaft-disk system. J Sound Vib 160(3):433–454
11. El-Marhomy AA (1997) Effect of various rotor-bearing system parameters on the whirl stability of system rotational modes of motion. Energy Convers Manag 38(1):73–82
12. Ryzhik B, Sperling L, Duckstein H (2004) Auto-balancing of anysotropically supported rotors. Tech Mech 24(1):37–50
13. El-Marhomy AA, Abdel-Sattar NE (2004) Stability of rotor-bearing systems via Routh-Hurwitz criterion. Appl Energy 77:287–308
14. Nelson HD, McVaugh JM (1976) The dynamics of rotor-bearing systems using finite elements. ASME J Eng Ind 98:593–600
15. Penny JET, Friswell MI, Lees AW, Garvey SD (2004) A simple but versatile rotor model. In: 8th international conference on vibrations in rotating machinery, Swansea (UK), September 7–9, pp 269–280
16. Rabinowitz MD, Hahn EJ (1977) Stability of squeeze-film damper supported flexible rotors. ASME J Eng Power 99:545–551
17. Rabinowitz MD, Hahn EJ (1977) Steady-state performance of squeeze-film damper supported flexible rotors. ASME J Eng Power 99:552–558
18. Kirk RG, Gunter EJ (1972) The effect of support flexibility and damping on the synchronous response of a single-mass flexible rotor. ASME J Eng Ind 94:221–232
19. Kirk RG, Gunter EJ (July 1972) Effect of support flexibility and damping on the dynamic response of a single-mass flexible rotor in elastic bearings, NASA CR-2083
20. Guo Z, Kirk RG (2003) Theoretical study on instability boundary of rotor-hydrodynamic bearing systems: Part I—Jeffcott rotor with external damping. ASME J Vib Acoust 125:417–422
21. Guo Z, Kirk RG (2003) Theoretical study on instability boundary of rotor-hydrodynamic bearing systems: Part II—Rotor with external flexible damped support. ASME J Vib Acoust 125:423–426
22. Liu LX, Spakovszky ZS (2007) Effects of bearing stiffness anisotropy on hydrostatic micro gas journal bearing dynamic behavior. ASME J Eng Gas Turbines Power 129:177 (8 pp)

23. Panda KC, Dutt JK (1999) Design of optimum support parameters for minimum rotor response and maximum stability limit speed. J Sound Vib 223(1):1–21
24. Panda KC, Dutt JK (2003) Optimum support characteristics for rotor-shaft system with preloaded rolling element bearings. J Sound Vib 260(4):731–755
25. Fischer J, Strackeljan J (2006) Stability analysis of high speed lab centrifuges considering internal damping in rotor-shaft joints. Tech Mech 26(2):131–147
26. Khulief YA, Mohiuddin MA (1997) On the dynamic analysis of rotors using modal reduction. Finite Elem Anal Des 26:41–55
27. Genta G (1988) Whirling of unsymmetrical rotors: a finite element approach based on complex coordinates. J Sound Vib 124(8):27–53
28. Genta G (2005) Dynamics of rotating systems. Springer, New York, pp 227–263
29. Sorge F, Cammalleri M (2009) An efficient damping technique for the unstable hysteretic rotor whirl by proper suspension systems. In: ECOTRIB 2009, Pisa, Italy, June 8–10
30. Crandall SH (1962) Rotating and reciprocating machines. In: Flügge W (ed) Handbook of engineering mechanics. McGraw–Hill, New York, pp 13–24 (Chap 58)
31. Wettergren HL (1997) On the behavior of material damping due to multi-frequency excitation. J Sound Vib 206(5):725–735
32. Nayfeh AH, Mook DT (1979) Nonlinear oscillations. Wiley, New York
33. Abramowitz M, Stegun IA (1964) Handbook of mathematical functions with formulas, graphs and mathematical tables. Applied mathematical series, vol 55. Nat. Bur. of Standards, U.S. Department of Commerce, Washington